Clays and Clay Minerals, Vol. 61, No. 4, 342–360, 2013.

THE INFLUENCE OF OXALATE-PROMOTED GROWTH OF SAPONITE AND TALC CRYSTALS ON RECTORITE: TESTING THE INTERCALATION-SYNTHESIS HYPOTHESIS OF 2:1 LAYER SILICATES

Dirk Schumann[1,*], Hyman Hartman[2], Dennis D. Eberl[3], S. Kelly Sears[4], Reinhard Hesse[1], and Hojatollah Vali[1,4]

[1] Department of Earth and Planetary Sciences, McGill University, 3450 University Street, Montreal, Quebec, H3A 0E8, Canada
[2] Department of Biomedical Engineering, MIT, Cambridge, MA 02139, USA
[3] U.S. Geological Survey, 3215 Marine St., Boulder, CO, USA
[4] Facility for Electron Microscopy Research, McGill University, 3640 University Street, Montréal, Québec, H3A 2B2, Canada

Abstract—The intercalating growth of new silicate layers or metal hydroxide layers in the interlayer space of other clay minerals is known from various mixed-layer clay minerals such as illite-smectite (I-S), chlorite-vermiculite, and mica-vermiculite. In a recent study, the present authors proposed that smectite-group minerals can be synthesized from solution as new 2:1 silicate layers within the low-charge interlayers of rectorite. That study showed how oxalate catalyzes the crystallization of saponite from a silicate gel at low temperatures (60ºC) and ambient pressure. As an extension of this work the aim of the present study was to test the claim that new 2:1 silicate layers can be synthesized as new intercalating layers in the low-charge interlayers of rectorite and whether oxalate could promote such an intercalation synthesis. Two experiments were conducted at 60ºC and atmospheric pressure. First, disodium oxalate solution was added to a suspension of rectorite in order to investigate the effects that oxalate anions have on the structure of rectorite. In a second experiment, silicate gel of saponitic composition (calculated interlayer charge −0.33 eq/$O_{10}(OH)_2$) was mixed with a suspension of rectorite and incubated in disodium oxalate solution. The synthesis products were extracted after 3 months and analyzed by X-ray diffraction and high-resolution transmission electron microscopy (HRTEM). The treatment of ultrathin sections with octadecylammonium (n_C = 18) cations revealed the presence of 2:1 layer silicates with different interlayer charges that grew from the silicate gel. The oxalate-promoted nucleation of saponite and talc crystallites on the rectorite led to the alteration and ultimately to the destruction of the rectorite structure. The change was documented in HRTEM lattice-fringe images. The crystallization of new 2:1 layer silicates also occurred within the expandable interlayers of rectorite but not as new 2:1 silicate layers parallel to the previous 2:1 silicate layers. Instead, they grew independently of any orientation predetermined by the rectorite crystal substrate and their crystallization was responsible for the destruction of the rectorite structure.

Key Words—Clay Minerals, High-resolution Transmission Electron Microscopy (HRTEM), Intercalation Synthesis, Lattice-fringe Images, *n*-alkylammonium Cations, Oxalate, Rectorite, Saponite, Talc, Smectite-group Minerals.

INTRODUCTION

The conversion of layer silicates through intercalation synthesis is a process that has been described for various groups of mixed-layer clay minerals such as illite-smectite (I-S), chlorite-smectite, chlorite-vermiculite, kaolinite-smectite, serpentine-chlorite, and mica-vermiculite (Gruner, 1934; Sudo *et al.*, 1954; Perry and Hower, 1970; Reynolds and Hower, 1970; Hower *et al.*, 1976; Brindley *et al.*, 1983; Dean, 1983; Ahn and Peacor, 1985; Moore *et al.*, 1989; Hughes *et al.*, 1993; Środoń, 1999). The intercalation of Mg-hydroxides into the interlayer space of 2:1 layer silicates such as smectite-group minerals or vermiculite-like minerals occurs in various geological environments, especially under weak hydrothermal conditions and is known as chloritization (Caillère and Hénin, 1949; Caillère *et al.*, 1953; Hénin and Robichet, 1954). The nature and origin of I-S mixed-layer clay minerals is still a matter of debate among clay mineralogists. During progressive burial-diagenesis, I-S mixed-layer clay minerals show an increase in the illite component in sedimentary basins throughout the world (Burst, 1959; Powers, 1967; Burst, 1969; Perry and Hower, 1972; Środoń and Eberl, 1984). Whether these minerals are truly interstratified crystals containing layers of two phases or whether they are physical stacks of two components which in X-ray diffraction (XRD) patterns mimic a single interstratified phase is still an open question (Hower *et al.*, 1976; Nadeau *et al.*, 1984, 1985; Ahn and Peacor, 1986; Bell, 1986; Sears *et al.*, 1995). Based on HRTEM investigations of I-S mixed-layer clay minerals after treatment with *n*-alkylammonium cations, Vali *et al.* (1994) suggested that the appearance of I-S mixed layers is

* E-mail address of corresponding author:
dirk.schumann@mail.mcgill.ca
DOI: 10.1346/CCMN.2013.0610413

related to the arrangement and composition of polar and non-polar 2:1 silicate layers, the polarity referring to the distribution of layer charges within the component sheets of the 2:1 layers.

The 2:1 layer silicate rectorite is described in the literature as a 1:1 ordered interstratification of dioctahedral mica layers and dioctahedral smectite layers (Bradley, 1950; Brindley, 1956; Brown and Weir, 1965; Henderson, 1970; Barron *et al.*, 1985a; 1985b). Other studies, however, have seen rectorite as a discrete 2:1 layer silicate composed of coherent sequences of polar T-O-T layers (Lagaly, 1979; Güven, 1991). A polar T-O-T (tetrahedral-octahedral-tetrahedral) 2:1 layer is characterized by two differently charged tetrahedral sheets sandwiching the octahedral sheet. One of the tetrahedral sheets has a larger and the other a smaller amount of isomorphous substitution of Si^{4+} by Al^{3+} causing differences in the layer charge. Thus, in a sequence of T-O-T layers opposite tetrahedral sheets of adjacent layers have alternating high or low degrees of Al^{3+} substitution resulting in alternating high-charge and low-charge interlayers. Jakobsen *et al*. (1995) were able to determine the composition of the octahedral and tetrahedral sheets of the mica-like and smectite-like layers and came to the conclusion that RAr-1 rectorite consists of paragonite-like and beidellite-like layers with the following balanced structural formulae (1) and (2):

paragonite: $(Na_{0.99}\ Ca_{0.07})(Al_{2.00}Fe^{3+}_{0.03}Mg_{0.01})[Al_{1.24}Si_{2.76}](OH)_2O_{10}$ (1)

and

smectite (beidellite): $R^+_{0.13}(Al_{2.00}Fe^{3+}_{0.03}Mg_{0.01})[Al_{0.24}Si_{3.76}](OH)_2O_{10}$, (2)

where R^+ represents exchangeable, monovalent interlayer cations like Na^+ and K^+. The following total structural formula for rectorite was proposed by Jakobsen *et al*. (1995):

$R^+_{0.12}(Na_{0.49}Ca_{0.01})(Al_{2.00}Fe^{3+}_{0.03}Mg_{0.01})[Al_{0.74}Si_{3.26}](OH)_2O_{10}$ (3)

The alternation of polar paragonite-like and beidellite-like T-O-T layers in rectorite forms a coherent sequence of 2:1 silicate layers with high-charge and low-charge interlayers.

Weiss (1981) described the intercalation synthesis of montmorillonite 2:1 silicate layers into the low-charge interlayers of the rectorite mineral, allevardite. According to that study the new montmorillonite layers grew from an aqueous solution that contained Na^+, K^+, Mg^{2+}, Al^{3+}, and $Si(OH_4)$ with a total electrolyte concentration of $\leqslant$0.02 N (Weiss, 1981).

In a recent study Schumann *et al*. (2012) synthesized saponite crystals from a silicate gel that was incubated in disodium oxalate solution. This study demonstrated how oxalate promoted the crystallization of saponite from a silicate gel at 60ºC and ambient pressure. The treatment of the synthesized saponite crystallites with octadecylammonium cations (n_C = 18) in combination with high-resolution transmission electron microscopy (HRTEM) imaging enabled the differentiation between single layers and packets of 2:1 layer silicates that have differently expanded interlayer spaces. The difference in interlayer expansion results from the variation in the substitution of Al^{3+} for Si^{4+} within the tetrahedral sheets of the saponite crystallites. The Si/Al ratio is passed on from one 2:1 silicate layer to the next within these little and highly expanded 2:1 silicate layer packets, as demonstrated by the regular interlayer expansion within the saponite packets. Therefore, the saponite 2:1 silicate layers may replicate by a template-catalyzed polymerization. The experimental results from the saponite synthesis experiment offered the opportunity to test the hypothesis of Weiss (1981). If the hypothesis is correct then the 2:1 silicate layers of saponite should replicate in the low-charge interlayers of rectorite.

In the present study, a different approach was used in order to investigate whether new smectite 2:1 silicate layers can be nucleated in the low-charge interlayer of rectorite. RAr-1 rectorite (for the source of the sample material see below) was added to a silicate gel with a chemical composition similar to saponite and reacted with disodium oxalate solution in a closed system at 60ºC and atmospheric pressure for 3 months.

If the intercalation synthesis occurs, it should be possible to document the existence of the newly generated saponite layers in HRTEM lattice-fringe images and by XRD analysis. Rectorite crystals composed of polar layers will react upon treatment with octadecylammonium (n_C = 18) cations and will appear as a sequence of 2:1 silicate layers with alternating expanded and non-expanded interlayers (Vali *et al.*, 1994; Sears *et al.*, 1998). Thus, if new layers of saponite grow within the low-charge interlayers of rectorite, observation of synthesized saponite layers within the expanded interlayers of rectorite after treatment with n_C = 18 cations should be possible.

MATERIALS AND METHODS

Experiments

The reference sample used in the present study was rectorite RAr-1 from the Source Clays Repository of The Clay Minerals Society. The saponite crystals were synthesized from a powdered silicate gel that was originally produced by Whitney (1983) according to the method outlined by Hamilton and Henderson (1968). The dried and powdered silicate gel was provided by C. G. Whitney. Expressed in weight percent oxide, the gel consisted of 56.25% SiO_2, 4.30% Al_2O_3, 30.88% MgO, and 3.97% K_2O.

The structural formula of saponite differs from other smectite-group minerals in that it has a positive charge emanating from the octahedral sheet that compensates

https://doi.org/10.1346/CCMN.2013.0610413 Published online by Cambridge University Press

partially for the negative charge from the tetrahedral sheet. The following structural formula for saponite

$$R^{n+}_{(x-y)/n}mH_2O\ (Mg_{3-y}R_y^{3+})\ (Si_{4-x}Al_x)(OH)_2O_{10} \quad (4)$$

from Brindley (1981) takes this positive octahedral charge into consideration where R^{3+} is mostly represented by Fe^{3+} and the interlayer space $R^{n+}mH_2O$ can be filled by hydrated Na^+, K^+, or Ca^{2+}. However, in systems without Fe^{3+}, the octahedral sheet may contain only Mg^{2+}, and, therefore, no positive charge arises from the octahedral sheet. The cation ratios of the silicate gel correspond to the following structural formula for saponite:

$$K_{0.33}Mg_3(Si_{3.67}Al_{0.33})(OH)_2O_{10} \quad (5)$$

Two experiments were set up which are referred to in the text as experiment 1 and 2. Experiment 1 contained 15 mL of rectorite suspension (<2 μm grain-size fraction) and 30 mL of 0.5 M disodium oxalate solution. The 0.5 M disodium oxalate solution was prepared from crystalline disodium oxalate powder ($Na_2C_2O_4$). This solution had a calculated pH of 8.98 at 25ºC. Experiment 2 was conducted using 315 mg of silicate gel powder, 15 mL of rectorite suspension, and 30 mL of 0.5 M disodium oxalate solution. The rectorite suspensions were prepared by adding 0.5 g of rectorite to 15 mL of distilled water. The starting pH of experiments 1 and 2 decreased gradually to 8.89 at 25ºC due to the addition of 15 mL of distilled water containing the rectorite suspension. Samples of experiments 1 and 2 were placed in tightly sealed centrifuge tubes (Oak Ridge style) and agitated constantly in an oven at 60ºC under atmospheric pressure for 3 months by using an end-over-end mixer.

XRD and TEM analysis

For XRD analysis, oriented air-dried samples were prepared by dispersing 50 mg of material in distilled water, transferring the suspension onto glass slides, and drying at room temperature for 24 h. After XRD analysis, the air-dried samples were solvated with ethylene glycol (EG) under its vapor pressure at 60ºC for 24 h and immediately re-analyzed by XRD. For *n*-alkylammonium intercalation, approximately 40 mg of dried material was placed in 1.5 mL polypropylene Eppendorf micro-test tubes and dehydrated with 100% ethanol for 24 h. After centrifugation the ethanol was removed and the samples were dispersed in a 0.05 M solution of octadecylammonium hydrochloride (n_C = 18) and left in an oven at 65ºC for 24 h. The following day, the samples were centrifuged, the old solution decanted, and the clay again dispersed in fresh 0.05 N octadecylammonium hydrochloride solution. This exchange procedure was repeated five times. After the fifth exchange the samples were washed at least 15 to 20 times with 100% ethanol to remove excess alkylammonium molecules and salts. The washed clay materials were dispersed in ~1 mL of 100% ethanol and pipetted onto glass slides, dried at room temperature, and X-rayed.

The XRD analyses of the air-dried and EG-solvated samples were performed on a Siemens D500 diffractometer at the USGS in Boulder, Colorado, USA. The XRD patterns of the samples treated with n_C = 18 solution were obtained using a Rigaku D/MAX 2400 12 kW rotating anode diffractometer at McGill University, Montreal, Quebec, Canada. At both locations CuKα radiation, a 0.02º step size, and a counting time of 2 s per step were used. Both of the systems were equipped with a graphite monochromator.

For HRTEM investigations, approximately 10–20 mg of the synthesized dried clay materials was placed in 1.5 mL polypropylene Eppendorf micro-test tubes and dehydrated by adding 100% acetone to remove adsorbed water. After high-speed centrifugation at a relative centrifugal force of $16{,}060 \times g$ for 15 min the supernatant was removed and the clay material dispersed in a mixture of 10% EPON resin and 90% acetone. These steps were repeated with mixtures containing 30%, 50%, 70%, and 100% EPON resin. In order to disperse the material the acetone resin mixtures were stirred and also agitated on an electrical shaker. Each incubation step lasted 24 h and during that time the samples were placed on a tilted rotating plate to ensure permanent agitation of the material. After the fifth incubation step (100% EPON resin), the resin-clay mixtures were transferred into embedding molds and left for polymerization at 65ºC for 48 h (Figure 1a,b; method 1). Ultrathin sections were cut from the resin blocks using an ultramicrotome and selected sections were transferred onto 300 mesh copper TEM grids with carbon support film (Figure 1c,d; method 1).

The n_C = 18 cation exchange treatment was carried out using a modified version of the procedure described by Vali and Hesse (1990). Each grid containing the ultrathin sections was placed face down in a 1.5 mL micro-test tube on the surface of the n_C = 18 solution diluted to 50% (0.025 M) (Figure 1e; method 1). The micro-test tubes were left for 20 min in an oven at 65ºC. The grids were removed from the tubes, held submerged in a Petri dish filled with 65ºC preheated distilled water, and agitated gently for several minutes in order to remove excess octadecylammonium hydrochloride solution or alkylammonium salts (Figure 1e; method 1). An additional subsample of the pure rectorite was treated with *n*-alkylammonium solution before the embedding in epoxy resin and cutting of the ultrathin sections (Figure 1; method 2). By comparing the lattice-fringe measurements of the expanded interlayers of rectorite, prepared according to methods 1 and 2, an answer to the question was possible as to whether the order of the *n*-alkylammonium-exchange treatment (before or after the embedding procedure) affects the expansion behavior of the rectorite.

All samples were studied in bright-field illumination mode at an acceleration voltage of 200 kV with a Philips CM200-TEM at the Facility for Electron Microscopy

https://doi.org/10.1346/CCMN.2013.0610413 Published online by Cambridge University Press

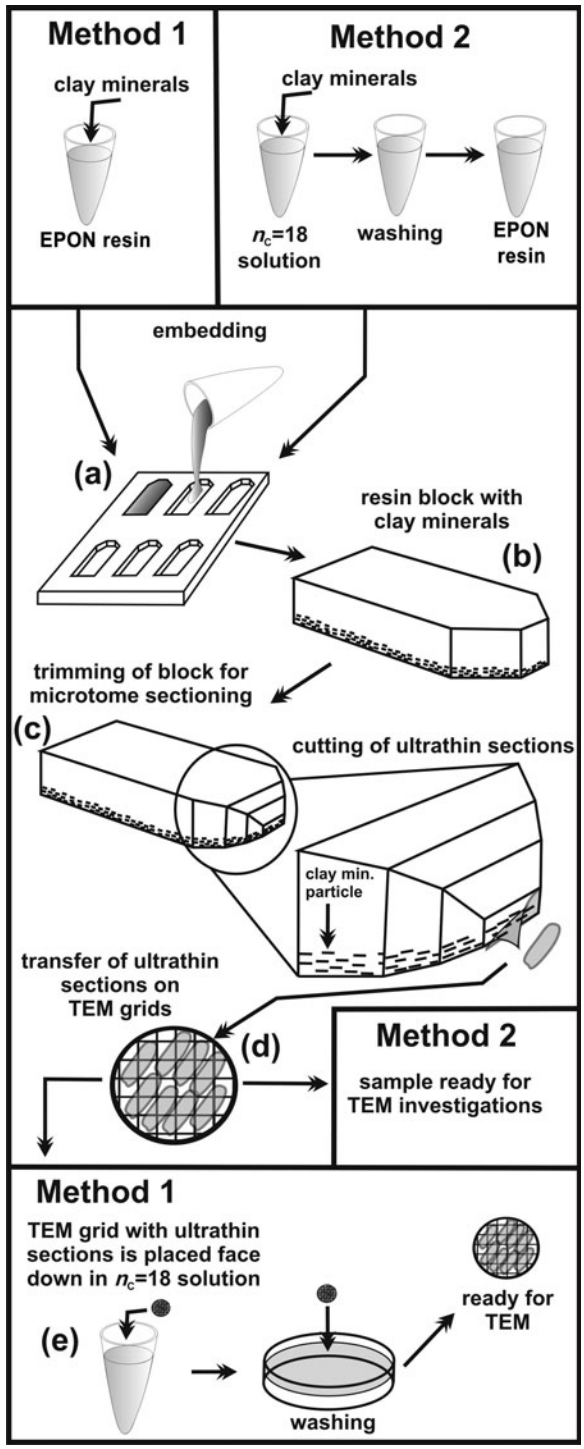

Figure 1. Sequence of drawings showing the final stage of the process of embedding clay minerals in epoxy resin, the preparation of ultrathin sections from these resin blocks, and the treatment of the ultrathin sections with *n*-alkylammonium cations for method 1. The *n*-alkylammonium cation-exchange procedure according to method 2 is conducted before embedding the clay material.

Research (FEMR) of McGill University. The TEM was equipped with an AMT CCD camera and an EDAX Genesis energy-dispersive X-ray spectroscopy system (EDS). Lattice-fringe images were taken at Scherzer defocus (underfocus) conditions (Vali *et al.*, 1991; Vali and Hesse, 1992).

The n-alkylammonium cation-exchange method

The *n*-alkylammonium cation-exchange method (Lagaly and Weiss, 1969) was developed for use as a tool in the determination of interlayer charge density, layer charge, and charge distribution in expandable 2:1 layer silicates such as smectite-group minerals, vermiculitic, and illitic minerals, based on XRD. An *n*-alkylammonium cation comprises an alkyl chain ($C n_C H 2n_C+2$) and an ammonium group (NH_3^+) with the general formula $C n_C H(2n_C+1)NH_3^+$, where n_C is the number of carbon atoms in the chain. During the exchange reaction the organic molecules replace the inorganic interlayer cations and expand the interlayer spacing of 2:1 clay minerals.

The degree of expansion is a function of the alkyl-chain length and the density of the interlayer charge. Alkylammonium cations having short- and intermediate-chain length ($6 \leqslant n_C \leqslant 11$) are capable of exchanging the inorganic interlayer cations of low-charge 2:1 layer silicates such as low-charge smectite-group minerals. Higher-charge 2:1 silicates like high-charge smectite group minerals, vermiculite, illite, glauconite, and the high-charge components of I-S undergo the cation exchange reaction in selected interlayers when treated with longer chains of alkylammonium cations ($12 \leqslant n_C \leqslant 18$). The *n*-alkylammonium cations also stabilize the expandable interlayers of 2:1 clay minerals under the vacuum of the TEM which otherwise would collapse if they contained only water or other organic molecules such as ethylene glycol or glycerol (Ahn and Peacor, 1986; Bell, 1986; Vali and Köster, 1986).

The arrangement of the alkylammonium cations within the 2:1 layer silicate interlayers depends upon the magnitude of the layer charge and the charge density. Low-charge smectite-group minerals have flat-lying monolayer (~13.6 Å), bilayer (~17.7 Å), or pseudotrimolecular (21.7 Å) arrangements while higher-charge smectite-group minerals, vermiculite-like minerals, expandable illites, or altered micas show paraffin-type arrangements of the *n*-alkylammonium cations (25–33 Å) (Figure 2) (Lagaly and Weiss, 1969; 1970a, 1970b, 1970c; Lagaly, 1981, 1982). Pseudotrimolecular arrangements may form in 2:1 layer silicates having a layer charge of >0.4 eq/$O_{10}(OH)_2$ whereas paraffin-type orientations of the alkylammonium chains occur at interlayer charges >0.63 eq/$O_{10}(OH)_2$ (Lagaly, 1982; Malla and Douglas, 1987; Lagaly and Dékany, 2005).

https://doi.org/10.1346/CCMN.2013.0610413 Published online by Cambridge University Press

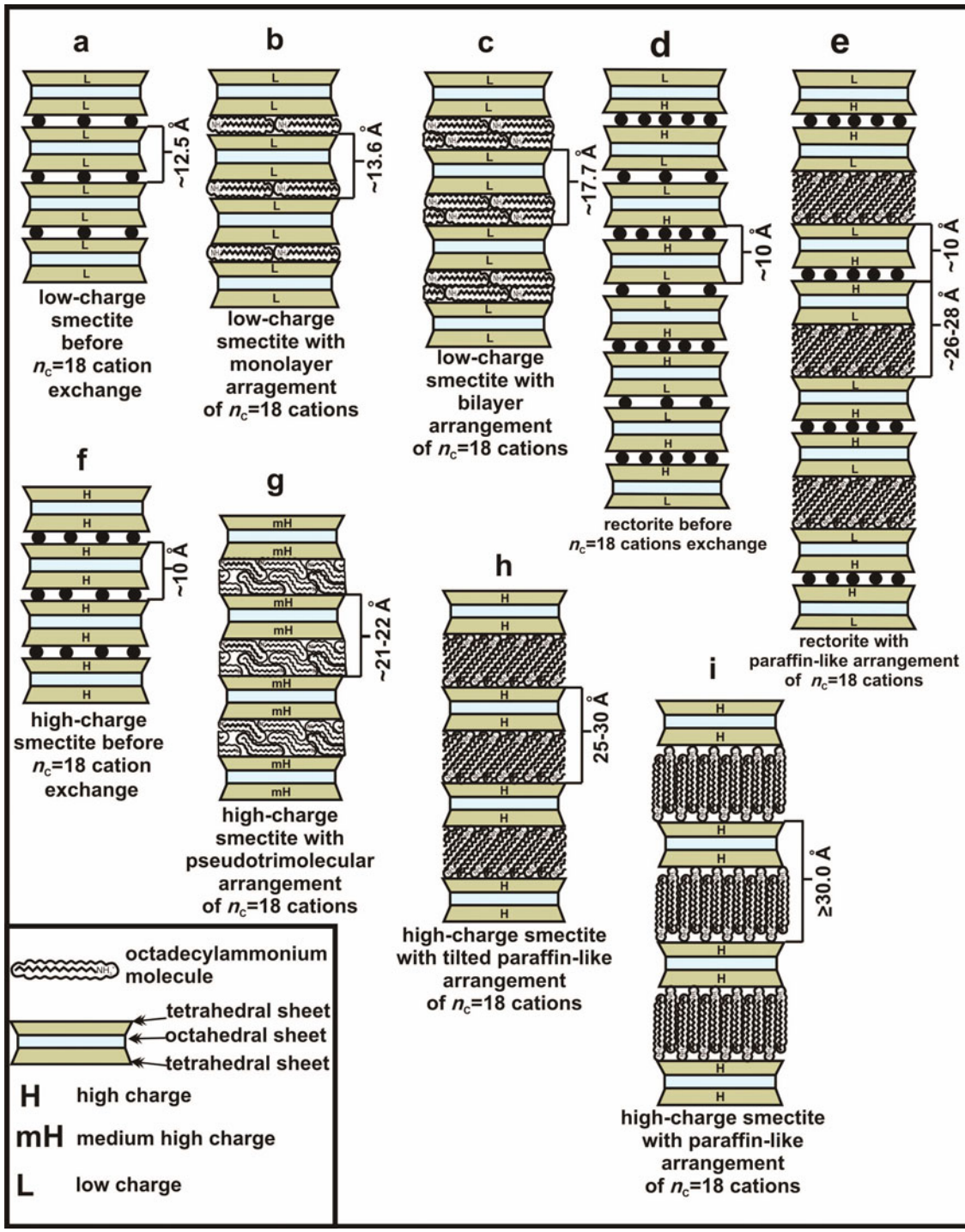

Figure 2. Models displaying the stacking order of polar and non-polar layers in 2:1 layer silicates before and after treatment with octadecylammonium (n_C = 18) cations (not to scale): (a) low-charge smectite-group mineral; (b,c) low-charge smectite-group mineral with monolayer (13.6 Å) and bilayer (17.7 Å) arrangements of the n_C = 18 cations; (d) rectorite; (e) rectorite after exchange with n_C = 18 cations consisting of alternating sequences of non-expanded (10 Å) and expanded (26–27 Å) interlayers; (f) high-charge smectite or vermiculite-like 2:1 layer silicates; (g) high-charge smectite-group or vermiculite-like 2:1 layer silicates with a pseudotrimolecular (21–22 Å) arrangement of n_C = 18 cations; and (h,i) paraffin-like arrangement of n_C = 18 cations with different tilt angles of the alkyl chains. Compilation of diagrams modified from Lagaly and Weiss (1969, 1970a, 1970b, 1970c), Lagaly (1981), Vali *et al*. (1994), and Shata *et al.* (2003).

https://doi.org/10.1346/CCMN.2013.0610413 Published online by Cambridge University Press

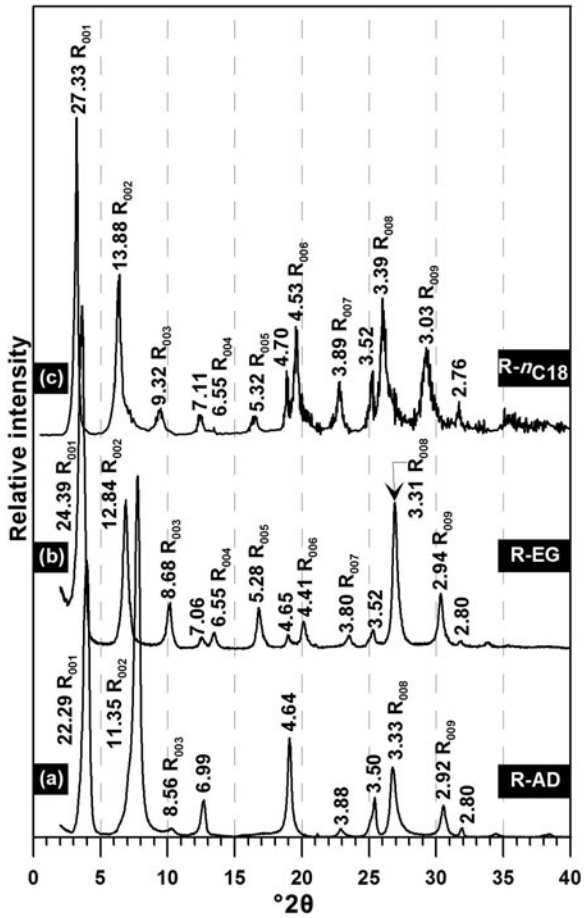

Figure 3. XRD patterns of the pure rectorite: (a) air-dried (AD); (b) ethylene glycol-solvated (EG); and (c) n_C = 18-treated pure rectorite. Reflections not indicated with an "R" (*i.e.* 7.11, 4.70, 3.52, 2.76) are non-integral reflections of rectorite. R – rectorite, n_C = 18 – octadecylammonium cations.

RESULTS

Pure rectorite

The XRD pattern of the air-dried rectorite has a first-order reflection at 22.29 Å which expands to 24.39 Å upon EG-solvation (Figure 3a,b). The XRD profile of the rectorite after treatment with n_C = 18 cations shows a sharp first-order reflection at 27.33 Å (001) and a set of integral reflections at 13.88 (002), 9.32 (003), 6.55 (004), 5.32 (005), 4.53 (006), 3.89 (007), 3.39 (008), and 3.03 Å (009) (Figure 3c). Transmission electron microscopy images of rectorite particles deposited from an

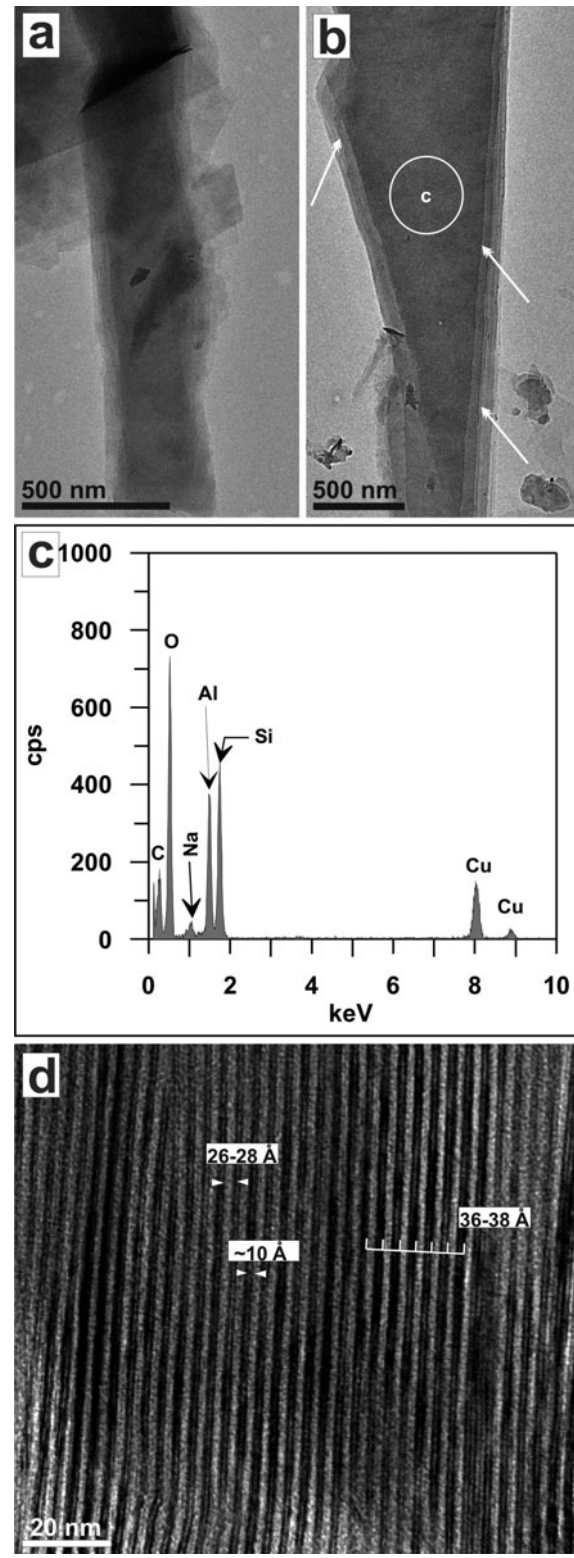

Figure 4 (*right*). (a) TEM image of a euhedral, ribbon-like rectorite particle. (b) Sub-euhedral to euhedral ribbon-like rectorite crystal (white arrows indicate growth steps). (c) EDS analysis of the area marked with a white circle in part b. (d) Lattice-fringe image of part of a rectorite crystal showing a sequence of alternating expanded (26–28 Å) and non-expanded (~10 Å) double layers. Non-expanded double layers and expanded layers together give a repeat unit of ~36–38 Å.

https://doi.org/10.1346/CCMN.2013.0610413 Published online by Cambridge University Press

aqueous suspension onto TEM copper grids showed euhedral, subhedral, and anhedral crystals. The subhedral and euhedral particles sometimes had a ribbon-like shape (Figure 4a,b). These crystals consisted of several layers that formed growth steps at the edges of the particle (Figure 4b: white arrows). The EDS analysis of a rectorite crystal showed high intensities for Si, Al, and O (Figure 4c). The interlayer cation Na appeared as a small peak around 1 keV. High-resolution lattice-fringe images of ultrathin sections of the rectorite after treatment with n_C = 18 cations showed alternating sequences of expanded layers (26–28 Å) and non-expanded layers (~10 Å) (Figure 4d).

Experiment 1: Rectorite and disodium oxalate solution

The XRD pattern of the oxalate-incubated rectorite failed to show the pattern of peaks which is typical of pure, air-dried rectorite (Figures 3, 5). The basal R_{001} diffraction of 20.43 Å was weaker and shifted toward higher 2θ angles (Figure 5a). The R_{002} reflection (10.20 Å) broadened and shifted toward higher 2θ angles. The R_{002} reflection was also significantly more intense than the R_{001} peak. A broad, low-angle shoulder appeared on the 4.67 Å reflection which was not visible in the pure rectorite (Figure 5a). The R_{008} integral reflection at 3.33 Å, clearly visible in the pure rectorite sample (Figure 3a), was very weak in the air-dried sample of the oxalate-incubated rectorite and coincided with a quartz reflection (Figure 5a). Instead, a strong reflection at 3.16 Å appeared in the oxalate-incubated rectorite (Figure 5a). The peak R_{009}, observable in the pure rectorite, was invisible in the air-dried sample of the incubated rectorite (Figure 5a). Peaks at 4.23 Å and 3.33 Å correspond to the 100 and 101 reflections of quartz. In addition to these changes, a small reflection at 13.80 Å appeared between the R_{001} and R_{002} basal reflections (Figure 5a). Upon EG-solvation and n_C = 18 treatment, the XRD patterns changed and were comparable with those of the pure rectorite. The small additional 13.80 Å reflection as well as the larger 10.20 Å and 3.16 Å peaks of the air-dried sample disappeared in the profiles of the EG-solvated and n_C = 18-treated samples (Figure 5b,c). High-resolution lattice-fringe images of the rectorite before n_C = 18 cation

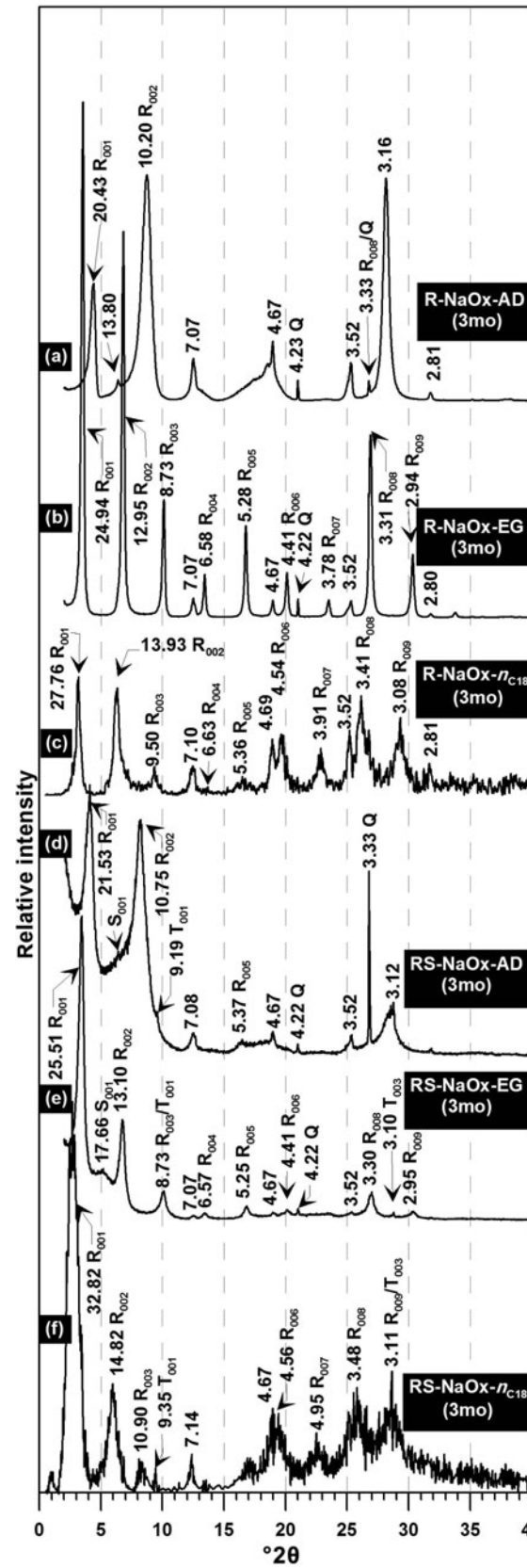

Figure 5 (*right*). XRD patterns of the rectorite incubated in disodium oxalate solution from experiment 1 and the synthesis product of experiment 2 containing rectorite, silicate gel, and disodium oxalate solution: (a) air-dried (AD); (b) ethylene glycol-solvated (EG); and (c) n_C = 18-treated rectorite that was incubated in oxalate solution. (d) AD, (e) EG-solvated, and (f) n_C = 18 treated synthesis products of experiment 3 (silicate gel, rectorite, and oxalate solution). Reflections marked with an 'R' are integral reflections of rectorite. R = rectorite. RS = rectorite-saponite mixture, S = saponite, T = talc, NaOx = disodium oxalate solution, n_C = 18 – octadecylammonium cations, 3mo = 3 months.

https://doi.org/10.1346/CCMN.2013.0610413 Published online by Cambridge University Press

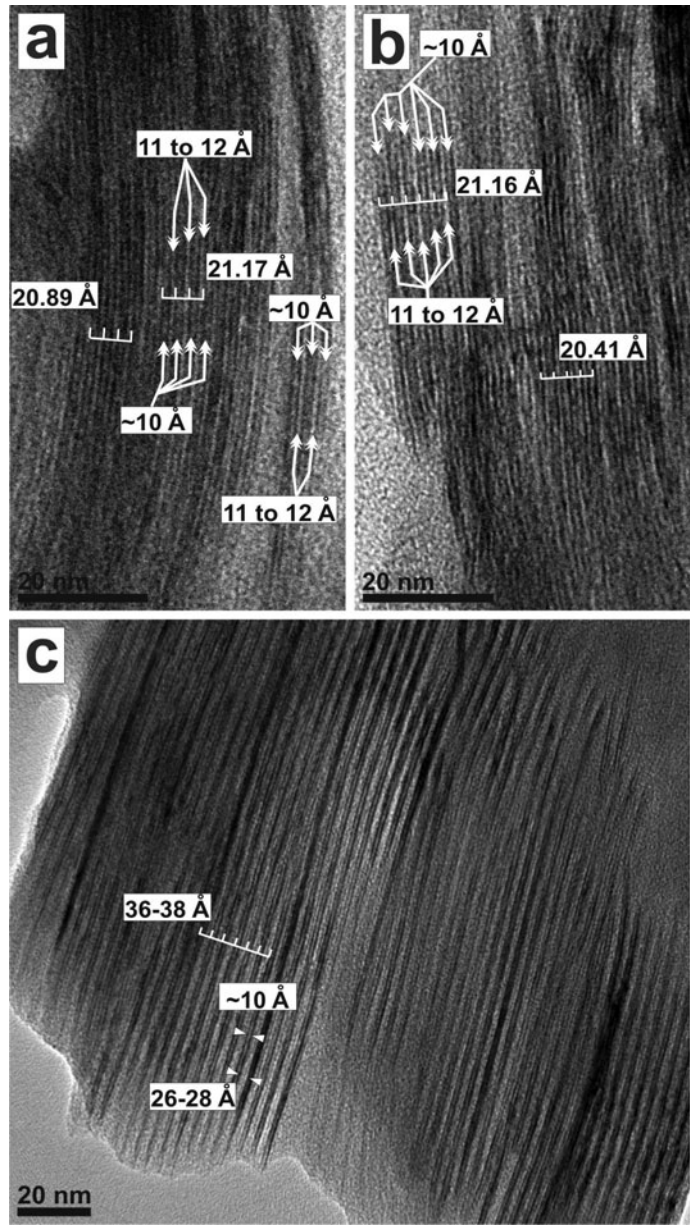

Figure 6. TEM images of rectorite incubated in disodium oxalate solution (experiment 1). (a,b) Lattice-fringe images of untreated rectorite crystals showing sequences of double layers with alternating spacings of ~10 and 11–12 Å. The same crystal also contains areas of 2:1 silicate layers in which former expandable layers have collapsed to values below 11 Å (*e.g.* value 20.41 Å = 10 Å + 10.41 Å; value 20.89 Å = 10 Å + 10.89 Å). (c) Lattice-fringe image of rectorite crystal after treatment with n_C = 18 cations showing a sequence of alternating expanded (26–28 Å) and non-expanded (~10 Å) layers.

treatment showed double layers with interlayer spacings of ~10 Å which alternated with interlayers with a spacing between 11 and 12 Å (Figure 6a,b). The same crystals also contained areas of 2:1 silicate layers in which the expandable layers collapsed to values of <11 Å (Figure 6a,b). The first-order reflection R_{001} of 20.43 Å suggests a value of 10.43 Å as the predominant spacing of the collapsed expandable layer (10.00 Å + 10.43 Å = 20.43 Å). Measurements in several lattice-fringe images gave values between 10.90 Å and 10.20 Å. For example, one sequence of lattice fringes that contained 10 Å layers and collapsed expandable interlayers gave values of 20.41 Å (10.00 Å + 10.41 Å = 20.41 Å) which is very close to the value (20.43 Å) obtained from the XRD pattern (Figure 6b). After treatment with n_C = 18 cations the rectorite incubated in disodium oxalate solution was comparable with the n_C = 18-exchanged pure rectorite that consisted of alternat-

https://doi.org/10.1346/CCMN.2013.0610413 Published online by Cambridge University Press

ing non-expanded double layers of ~10 Å and expanded double layers of 26–28 Å spacings (Figure 6c).

Experiment 2: silicate gel, rectorite, and disodium oxalate solution

By comparing the XRD patterns of pure rectorite with those of the experiment containing silicate gel, rectorite, and disodium oxalate solution, differences in the AD XRD traces were apparent (Figures 3a, 5d). The basal R_{001} and R_{002} diffractions of rectorite shifted toward higher 2θ angles (Figure 5d). The S_{001} basal reflection of the saponite component interfered with the R_{002} reflection of rectorite causing a broad low-angle shoulder on that peak (Figure 5d). The clearly visible peak at 4.64 Å in the pure rectorite appeared as a very weak reflection at 4.67 Å in the rectorite/silicate gel mixture (Figures 3a, 5d). The R_{008} integral reflection at 3.33 Å, well represented in the pure rectorite sample, did not appear in the oxalate-incubated rectorite/silicate gel mixture (Figures 3a, 5d). However, at the same position (3.33 Å) the sharp 100 reflection of quartz appeared. The AD sample of the rectorite/silicate gel mixture also showed a 3.12 Å reflection which was not visible in the pure AD rectorite XRD profile (Figures 3a, 5d). The T_{001} reflection of a talc-like phase was visible as a small peak at the high-angle shoulder of the R_{002} reflection (Figure 5d).

Upon EG solvation the reflections of the rectorite and saponite components became better resolved from each other. The rectorite component had similar peak positions to those of the pure rectorite (Figures 3b, 5e). The S_{001} peak of the saponite component had a first-order reflection at 17.66 Å and appeared between the R_{001} and R_{002} reflections in the EG-solvated sample (Figure 5e).

The pattern changed significantly after the sample was treated with n_C = 18 cations. A broad, first-order peak R_{001} of the rectorite structure appeared at 32.82 Å (Figure 5f). The peaks of this pattern were broader than in the EG-solvated sample and shifted toward lower 2θ angles (Figure 5f). This is unusual as one would expect patterns similar to the EG-solvated XRD traces but with sharper and more intense reflections. The S_{001} basal reflection of the saponite component was unresolved from the rectorite pattern. Instead, it was responsible for the broadening of the R_{002} reflection toward lower angles (Figure. 5f). The R_{003} reflection of rectorite and the T_{001} peak of the talc-like phase became separated. The R_{008} and R_{009} reflections also shifted toward lower 2θ angles. Detailed HRTEM and XRD characterizations of the saponite crystals that were synthesized from the same powdered silicate gel in the presence of 0.5 M disodium oxalate solution were published in Schumann *et al*. (2012). They showed XRD patterns of the pure silicate gel, the air-dried, EG-solvated, and the n_C = 18 cation-treated synthesized saponite (Figure 7). The saponite had a S_{001} basal reflection at 17.76 Å after exchange with n_C = 18 cations (Figure 7d).

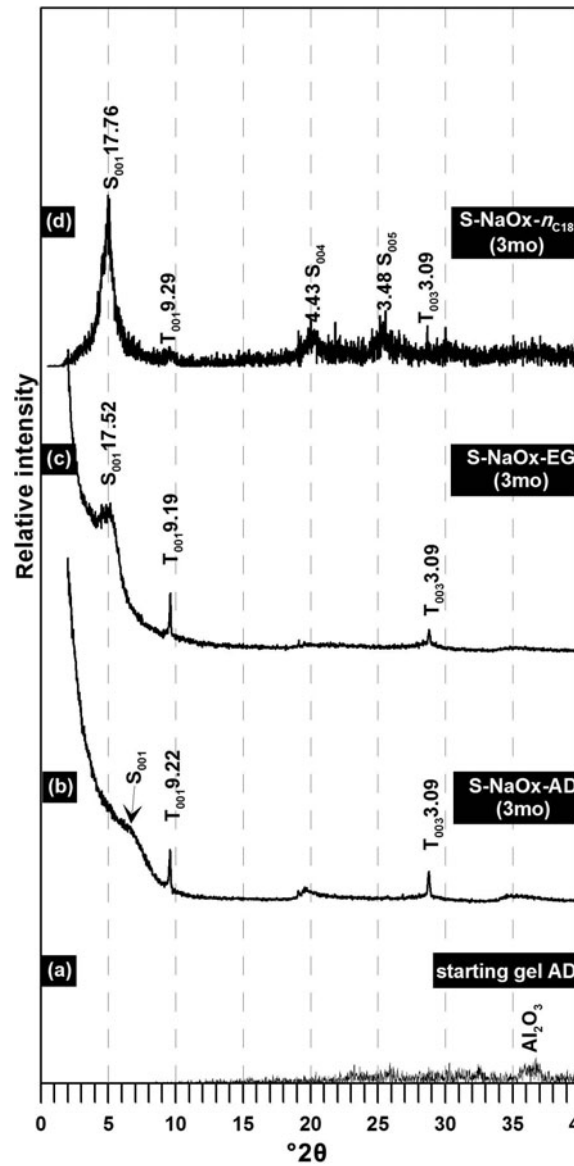

Figure 7. XRD patterns of saponite synthesized from the same silicate gel as in the present study in the presence of disodium oxalate solution (from Schumann *et al*., 2012): (a) air-dried (AD) starting silicate gel; (b) air-dried (AD) saponite; (c) ethylene glycol-solvated (EG) saponite; and (d) n_C = 18-treated saponite. S = saponite, T = talc, NaOx = disodium oxalate solution, n_C = 18 – octadecylammonium cations, 3mo = 3 months.

The TEM images of the synthesis products showed subhedral to euhedral rectorite crystals, globular aggregates of saponite, and an overgrowth of talc crystallites on rectorite (Figure 8a,b,d,e,f,g). Rectorite crystals with different stages of alteration were also seen. The edges of the rectorite crystals acted as nucleation sites for crystallites of talc. They were mantled by a talc overgrowth in various stages of crystallization. Some were only surrounded by a minor rim of small flakes

https://doi.org/10.1346/CCMN.2013.0610413 Published online by Cambridge University Press

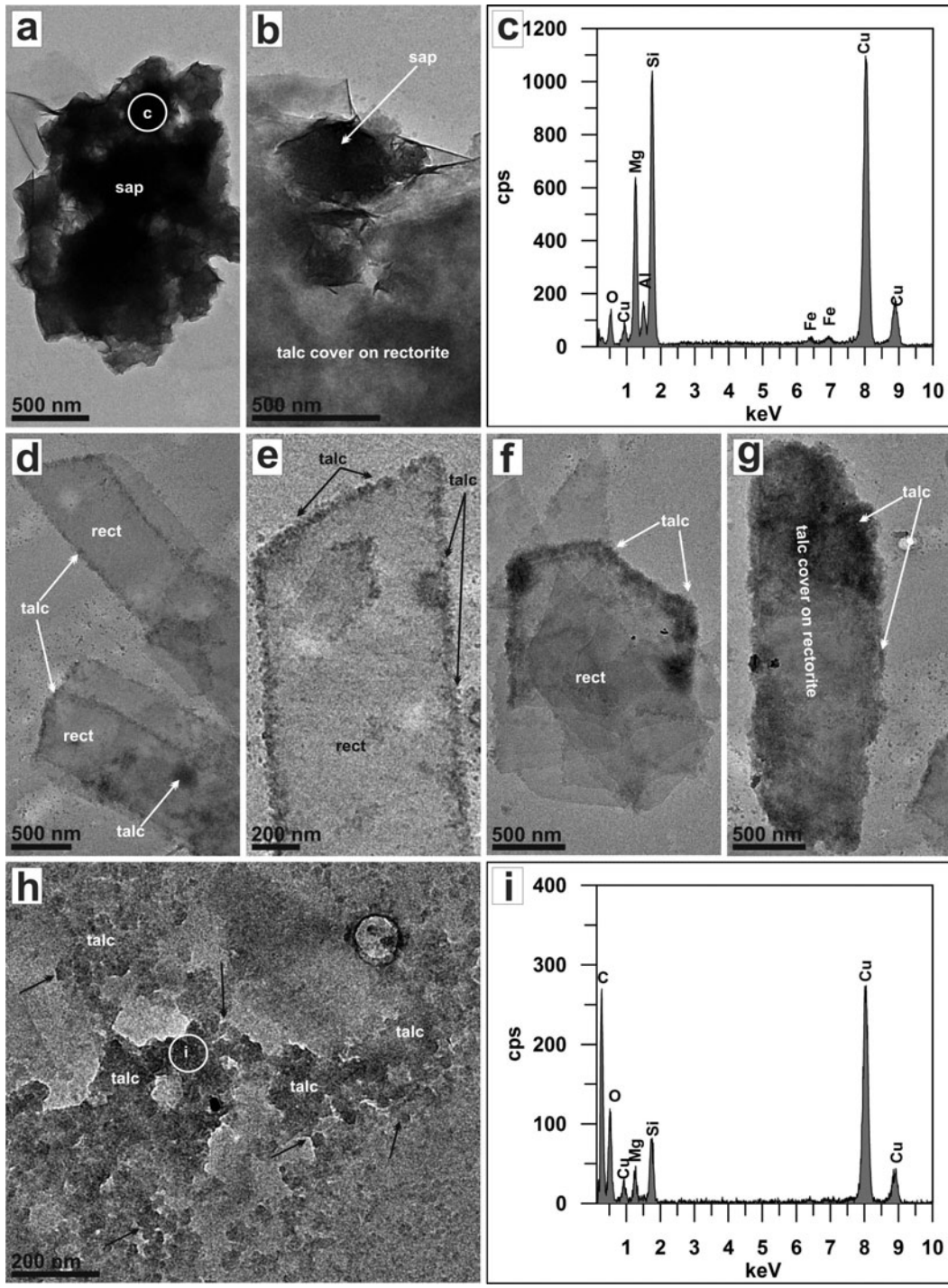

Figure 8. TEM overview images of the synthesis products of experiment 2 (silicate gel + rectorite + disodium oxalate solution): (a) globular aggregates of saponite crystallites (sap); (b) globular aggregate of saponite crystallites (sap) which grows in an altered edge zone of a rectorite crystal. The rectorite crystal itself is covered completely with a fine, newly crystallized talc overgrowth (cloudy grayish mass). (c) EDS analysis of the globular aggregate of saponite from part a; (d,e) euhedral rectorite crystals (rect) with fine overgrowth of newly formed talc crystallites along their edge sites; (f) rectorite crystal in the center shows an advanced overgrowth of talc starting from the edge sites of the crystal; (g) strongly altered rectorite crystal completely covered with talc overgrowth; (h) talc crystallites (black arrows) on the surface of the carbon film of the TEM grid; and (i) EDS analysis of the area with talc crystallites indicated by a white circle in part h. The Cu peak is due to the copper grid. The C peak is caused by the carbon support film of the TEM grid.

https://doi.org/10.1346/CCMN.2013.0610413 Published online by Cambridge University Press

while others showed an advanced stage of overgrowth (Figure 8d,e,f,g). In some cases, the crystallization of globular aggregates of saponite was observed within strongly altered areas of rectorite crystals (Figure 8b). Fine crystallites of talc also appeared as diffuse and cloudy masses on the planar (001) crystal surfaces of rectorite (Figure 8b,d,g). The EDS analyses of the saponite globules showed large Si and Mg contents but a small Al content which is typical of the synthesized saponite (Figure 8c). Elemental analyses of the fine talc crystallites that grow on the edges and the planar (001) surface of the rectorite indicated the presence of Mg and Si only, which confirmed that these crystals were not saponite (Figure 8h,i).

Lattice-fringe images of the ultrathin sections treated with n_C = 18 cations documented the alteration of rectorite and the crystallization of saponite and talc. Based on the expansion behavior of the saponite, two structures were identified in the lattice-fringe images. Sequences and packets with interlayer spacings of 25−33 Å were the predominant phase (Figure 9a,c,f: white diamonds) while curved or planar sequences of 2:1 layer silicates having an interlayer spacing between 13 and 14 Å appeared as minor phases (Figure 9b,e,f: white half circle). Lattice-fringe images also showed clusters of disorganized single silicate layers of talc (Figure 9c,d,e: white circle). Rectorite crystals both appeared as unaltered large sequences similar to those described in the pure rectorite and as altered sequences (Figure 9c-g). The expandable rectorite interlayers in the unaltered center of the rectorite sequences have spacings similar to those measured in pure rectorite (26−28 Å) (Figures 3d, 9c,d). Alteration features were associated with the areas of talc and saponite crystallization. The newly crystallized talc and saponite split the rectorite structure apart starting from the edges of the rectorite and proceeding along the low-charge interlayers (expandable interlayers) of the rectorite sequences (Figure 9c−e). This led to the expansion of these interlayers to up to 44 Å and also to the disruption of the large crystals into shorter sequences (Figure 9b−g). The high-charge 10 Å double layers failed to split apart. In an advanced stage of alteration only dispersed single ~10 Å double layers were left behind from a former coherent rectorite sequence (Figure 9g: black arrows).

DISCUSSION

Experiment 1: rectorite and disodium oxalate solution

Numerous studies have investigated the effects of organic-acid anions, including oxalate, on the dissolution rates of minerals, with the result that organic-acid anions have a much larger effect on Al-rich minerals than on minerals which contain little or no Al. This is due to the apparent preferential adsorption of oxalate on Al sites and the resulting ligand-promoted dissolution (Boyle *et al.*, 1967; Surdam and MacGowan, 1978; Bevan and Savage, 1989; Stoessell and Pittman, 1990; Fein, 1991; Fein and Hestrin, 1994; Fein and Brady, 1995; Blake and Walter, 1996; Welch and Ullman, 1996; Stillings *et al.*, 1998; Axe and Persson, 2001). In particular, mineral surface complexation and dissolution involving the oxalate species $HC_2O_4^-$ and $C_2O_4^{2-}$ between 20 and 100ºC have been the subject of various studies (Fein, 1991; Tait *et al.*, 1992; Thyne *et al.*, 1992; Fein and Hestrin, 1994; Fein and Brady, 1995; Blake and Walter, 1996; Axe and Persson, 2001). The hydrolysis of disodium oxalate in water proceeds according to the following equations:

$$Na_2C_2O_4 \rightarrow 2Na^+ + C_2O_4^{2-} \quad (6)$$

$$C_2O_4^{2-} + H_2O \rightarrow HC_2O_4^- + OH^- \quad (7)$$

Bonding of carboxylate and oxalate species commonly occur through inner-sphere complexation with a direct bonding to the surface cations at the edge sites, *e.g.* Al^{3+} and/or outer-sphere complexation where the organic anion is held by hydrogen bonds and electrostatic forces (Dobson and McQuillan, 1999; Axe and Persson, 2001; Duckworth and Martin, 2001; Sherman and Randall, 2003; Yoon *et al.*, 2004). Aside from the surface reactions that might take place, the disodium oxalate solution also seems to affect the structure of the rectorite as documented in the XRD patterns of the air-dried samples through changes in peak position and the appearance of new peaks (Figure 5a). The AD rectorite incubated in disodium oxalate for 3 months has an R_{001} reflection at 20.43 Å (Figure 5a). The R_{002} reflection becomes dominant and shifts toward 10.20 Å (Figure 5a). The HRTEM lattice-fringe images of embedded air-dried material show areas within the crystals that still contain alternating sequences of non-expanded layers (~10 Å) and expandable layers (11−12 Å). However, in many areas of a sequence the expandable layers have collapsed to values <11.0 Å (10.90−10.20 Å) (Figure 6a,b). Upon treatment with EG or n_C = 18 cations the dominant reflection at 10.20 Å disappears. The cation exchange reaction with organic molecules generates the typical XRD pattern for rectorite. This observation suggests that excess Na^+ is first incorporated into the interlayer space of the low-charge layers causing a contraction of the structure and the development of a first-order reflection close to 10.20 Å. After treatment with EG or n_C = 18 cations, the Na^+ of the low-charge interlayers is replaced by the organic molecules and the rectorite XRD pattern is similar to those of the EG- or n_C = 18-exchanged pure rectorite.

The additional small reflection at 13.80 Å between the rectorite R_{001} and R_{002} reflections in the AD sample (Figure 5a) suggests the formation of hydroxy-Al complexes probably intercalated in some of the expandable rectorite interlayers as discontinuous 'gibbsite-like' sheets. MacEwan (1949) first described 2:1 layer silicates with intercalated hydroxy-Al interlayers from

https://doi.org/10.1346/CCMN.2013.0610413 Published online by Cambridge University Press

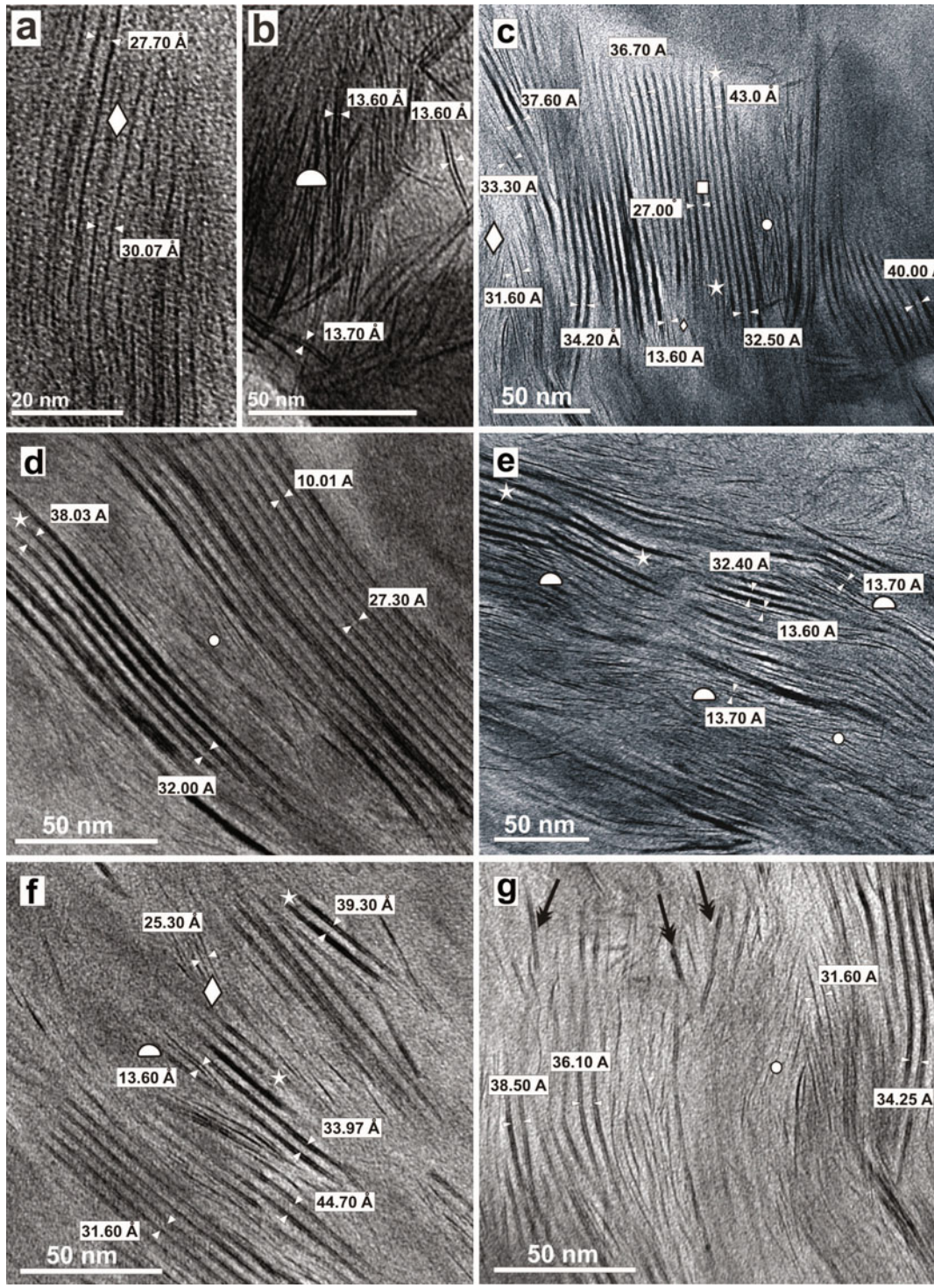

Figure 9. Lattice-fringe images of n_C = 18-treated experimental mixtures of silicate gel, rectorite, and disodium oxalate solution (experiment 2): (a) lattice-fringe images of synthesized saponite crystals with curved to planar 2:1 silicate layers having expanded interlayer spacings that range from ~25 Å to ~33 Å (white diamond); (b) short sequences of two to four saponite 2:1 silicate layers with a spacing of between 13 and 14 Å (white half circle); (c) lattice-fringe image showing an altered rectorite crystal consisting of non-expanded double layers of ~10 Å alternating with expanded double layers that range from ~ 27 Å (white squares) in the center of the sequence to up to 40 Å (white stars) at the edges of the crystal; (d) short sequence of altered rectorite crystals that were split apart through the growth of the talc and saponite crystals (white circle); (e,f,g) areas containing heavily altered rectorite crystals and newly formed talc (white circles) and saponite crystallites (white half circles and white diamonds).

https://doi.org/10.1346/CCMN.2013.0610413 Published online by Cambridge University Press

soils. They contain incomplete Al-chlorite layers. In the air-dried state they show a reflection around 14 Å-like chlorite. However, upon treatment with swelling agents, they showed a smectite- or vermiculite-like behavior suggesting that the hydroxy-Al sheet does not prevent exchange with organic molecules and, hence, the swelling of the interlayer (Rich, 1968; Barnhisel and Bertsch, 1989; Meunier, 2007).

Other studies have reported mixed-layer illite/Al-hydroxy vermiculites as weathering products in soils (Farmer *et al.*, 1988; Bain *et al.*, 1990). In XRD patterns, these clay minerals, in addition to the major vermiculite and illite reflections of ~24.7 Å and 10 Å, showed peaks similar to chlorite minerals between 14.2 Å and 14.5 Å which do not change position upon EG-solvation. These Al-hydroxy interlayers have been suggested to form in 2:1 layer silicates in soil due to the activity of organic complexes which transport Al. The decomposition of the organic Al complexes increases the pH and results in the precipitation of hydroxy-Al (April *et al.*, 1986). Therefore, one may assume that in experiment 2 the oxalate anions formed complexes with the Al at the edges of the rectorite crystals and probably caused partial dissolution of the crystals, making Al available for the formation of Al-hydroxy interlayers.

Upon treatment with EG or n_C = 18 cations, the small peak at 13.80 Å also disappeared in the XRD pattern (Figure 5b,c). This may be due to the fact that the organic molecules exchange the Al-hydroxy octahedral sheets in the interlayer causing the XRD pattern to look like those of EG-solvated or n_C = 18-treated pure rectorite (Figures 3b,c and 5b,c). These observations are supported by lattice-fringe images taken from the n_C = 18-treated samples that show similar sequences to pure rectorite but show no Al-hydroxy layers in the expanded rectorite interlayers (Figures 4d, 6c). The intercalation synthesis of Al-hydroxy layers in certain rectorite interlayers is based on evidence obtained from XRD patterns. Lattice-fringe images provided no evidence for this interpretation.

Experiment 2: silicate gel, rectorite, and disodium oxalate solution

The XRD pattern of the sample material exchanged with n_C = 18 cations shows the broadening of the first-order R_{001} diffraction suggesting the opening or destruction of the large rectorite sequences along the low-charge interlayers. This was confirmed through both low-magnification TEM images and the HRTEM lattice-fringe images of the n_C = 18-exchanged ultrathin sections (Figures 8, 9). The TEM images of the untreated suspension showed single aggregates of saponite crystals but also rectorite crystals that act as nucleation sites for aggregates of saponite crystallites (Figure 8a,b). Rectorite crystals also act as nucleation sites for talc. Most of the rectorite crystals have their edge sites covered by newly formed talc crystallites (Figure 8d–f); others are completely covered with talc (Figure 8g). Charges at the edges cause the mobilized ions from the silicate gel to bind and subsequently form T-O-T nuclei of talc according to the edge-site nucleation model proposed by White and Zelazny (1988). These new talc crystallites act as nucleation sites for additional talc crystals which finally cover the entire rectorite particles and also intrude into the low-charge interlayers causing the disruption of the sequences (Figure 8d–g, 9c–g). The alteration features of the rectorite sequences can be observed in lattice-fringe images in areas that show saponite and talc crystal growth, while zones without saponite or talc crystallites show intact rectorite sequences. The saponite and talc crystallites grow irregularly into the expandable rectorite interlayers causing the sequences to split apart as seen in the samples treated with n_C = 18 cations (Figure 9c–g).

Two processes may explain the changes observed both in the XRD patterns and TEM images: (1) the crystallization of saponite and talc crystallites from the gel; and (2) the subsequent alteration of the rectorite structure leading to its ultimate disruption. The crystallization reaction of saponite and talc can be written as follows:

saponite:

$$0.33\ K^+ + 3.67\ SiO_2 + 0.33\ Al(OH)_3 + 3\ Mg(OH)_2 \leftrightarrow K_{0.33}\ Mg_3(OH)_2(Si_{3.67}\ Al_{0.33})O_{10} + 0.33\ H^+ + 2.33\ H_2O \quad (8)$$

talc:

$$4\ SiO_2 + 3\ Mg(OH)_2 \leftrightarrow Mg_3Si_4O_{10}(OH)_2 + 2H_2O \quad (9)$$

The saponite crystallization reaction is associated with the release of protons into the solution that should lead to the decrease in the pH. While rectorite is more or less stable at a neutral to alkaline pH and a temperature of 60ºC, it probably starts to dissolve at pH <7 in the same way that illite does at similar temperatures (Koehler *et al.*, 2003). The dissolution reaction may be further enhanced in the presence of oxalate and its tendency to form complexes with Al. The oxalate complexes can be considered stable under the experimental conditions of 60ºC and atmospheric pressure (Couturier *et al.*, 1984; Fein, 1991; Tait *et al.*, 1992) as the thermal degradation of aqueous oxalate species to formic acid, CO_2, and H^+ occurs at much higher temperatures and is favored by a low pH (Crossey, 1991). Therefore, the major source of protons that could reduce the pH in experiment 2 is the crystallization reaction of saponite. Unfortunately, final pH measurements were not done and, therefore, this hypothesis cannot be tested. However, it is possible that the combination of proton release through saponite nucleation, the crystallization of talc and saponite on the rectorite itself, as well as the formation of oxalate complexes on the rectorite surface, could be responsible for the destabilization and dissolution of the rectorite crystals. The destruction of the rectorite sequences by dissolution as well as the irregular growth of saponite

https://doi.org/10.1346/CCMN.2013.0610413 Published online by Cambridge University Press

and talc crystallites within the expandable interlayers of the rectorite causes the opening of these interlayers and is responsible for the peak broadening and the migration of the first-order reflection of rectorite R_{001} towards lower 2θ values in the XRD patterns of the EG-solvated and n_C = 18-exchanged samples.

The results of these experiments showed no evidence of intercalation synthesis of new saponite layers within the low-charge interlayer of rectorite. In the present experiments, the low-charge interlayer of rectorite did not act as a seed or a template for the synthesis of new saponite layers. Instead, the saponite crystallites that grew from the silicate gel formed single layers, packets, or bundles independent of the orientation of the rectorite T-O-T layers.

Discrepancy between d values obtained from XRD and from TEM lattice-fringe images

The evaluation of the lattice-fringe images of the synthesized saponite, the rectorite, and the saponite-rectorite mixtures reveal discrepancies between layer-spacing measurements taken in lattice-fringe images and those obtained from XRD patterns.

Saponite. Lattice-fringe images of the n_C = 18-cation exchanged synthesized saponite show the predominance of highly expanded interlayers of 25–33 Å and a minor amount of double layers or packets with spacings between 13 and 14 Å. The latter have a monolayer arrangement of n_C = 18 cations while a paraffin-like intercalation of n_C = 18 cations is responsible for highly expanded interlayers with 25–33 Å spacings (Figures 2b,h,i, 8a,b). The existence of differently expanded saponite crystallites as shown in the lattice-fringe images suggests the crystallization of T-O-T layers with different levels of Al^{3+} substitution in the tetrahedral sheets, resulting in a smaller or larger negative charge of these layers. The variation of the interlayer spacing is a direct result of differences in interlayer charge, which in turn reflects the amount of isomorphous substitution within the T-O-T layers. The analysis of lattice-fringe images enables the distinction between individual packets of saponite crystallites with different interlayer charge values and of charge differences even within single 2:1 silicate layers.

The structural formula derived from the chemical composition of the silicate gel has an interlayer charge of −0.33 eq/$O_{10}(OH)_2$. The presence of differently expanded saponite crystallites suggests that the synthesis process did not form only saponite crystals with a single homogeneous interlayer charge of −0.33 eq/$O_{10}(OH)_2$; but, instead, at least two different structures were formed. The present study cannot determine whether the sequences of highly expanded saponite crystals have an interlayer charge of exactly −0.33 eq/$O_{10}(OH)_2$ or whether the values are slightly higher or lower. However, it can be inferred that the sequences of highly expanded saponite layers (25 to 33Å) have greater interlayer charge than those of the 2:1 silicate layer sequence with spacings of between 13 and 14 Å.

X-ray diffraction analysis of the saponite synthesized from the same silicate gel in the presence of disodium oxalate solution (by Schumann *et al*., 2012) suggested the predominance of 2:1 layer silicates with a bilayer arrangement of n_C = 18 cations and an expansion of 17.76 Å (Figure 7d) which is different from the observations made in HRTEM lattice-fringe images (see also figures 2 and 4 of Schumann *et al*., 2012). The predominant, highly expanded 25–33 Å saponite structures as seen in the lattice-fringe images correspond to the 17.76 Å bilayer structures from the XRD pattern (Figure 9a of the present study and figure 4 of Schumann *et al*., 2012). The highly expanded structures observed in lattice-fringe images are caused by the additional incorporation of *n*-alkylammonium cations due to the high concentration of the exchange solution (0.025 M) and the nature of the washing procedure that does not guarantee the removal of all excess alkylammonium molecules (Schumann *et al*., 2012).

The cross-sectional areas of the clay-mineral aggregates in the ultrathin sections were exposed to the *n*-alkylammonium solution during the exchange procedure (Figure 1e). The exchange reaction contains two basic steps. First, all exchangeable inorganic interlayer cations are replaced by *n*-alkylammonium cations expanding the 2:1 clay-mineral structures according to their layer charge. After that, a second reaction can take place in which pairs of *n*-alkylammonium molecules enter the interlayer space and are held there through van der Waals interactions (He *et al*., 2004, 2005, 2006). This conclusion is supported by several studies that investigated the effect of different concentrations of hexadecyltrimethylammonium (HDTMA) solution on the expansion behavior of montmorillonite (Lee and Kim, 2002; Zhu *et al*., 2003; He *et al*., 2004). These studies have shown that with the increase in the concentration of surfactant beyond the cation exchange capacity of the clay minerals, the intercalation of the HDTMA molecules will change from monolayer to bilayer arrangement and then to mono- and bilayer paraffin-type arrangements.

Unfortunately, the CEC of the synthesized saponite could not be measured due to the insufficient amount of sample material. However, the significant degree of expansion of the 2:1 silicate layers of the saponite crystals infers that the concentration (0.025 M) of the n_C = 18 solution used for the cation exchange reaction was certainly greater than the CEC of the saponite crystals. After the treatment with n_C = 18 cations, the ultrathin sections were washed gently with preheated distilled water which was obviously insufficient to achieve complete removal of all excess alkylammonium molecules from the interlayer space. Therefore, the crystals with excess n_C = 18 cations in the interlayer space

https://doi.org/10.1346/CCMN.2013.0610413 Published online by Cambridge University Press

appear in lattice-fringe images as very expanded sequences of 2:1 silicate layers (25–33 Å). Ethanol, which is used as a washing solution for the removal of excess *n*-alkylammonium molecules from XRD samples, is not applicable for the washing of ultrathin sections as the ethanol would dissolve the epoxy resin of the sections and would cause the loss of clay-mineral crystals.

The duration of the *n*-alkylammonium cation-exchange procedure also affects the arrangement of intercalated *n*-alkylammonium cations and, therefore, the expansion behavior of the saponite 2:1 silicate layers. The 2:1 silicate layers with a 13–14 Å spacing have a monolayer arrangement of the alkylammonium molecules in their interlayer spaces. The interlayer charge density is low and, therefore, the *n*-alkylammonium chains have sufficient space to arrange themselves as flat-lying monolayers. According to Maes *et al.* (1979) the transition from a monolayer (13.6 Å) to a bilayer (17.7 Å) arrangement only occurs if the layer charge of 2:1 layer silicates is >0.24eq/$O_{10}(OH)_2$. This is the case for most of the synthesized saponite crystals as the XRD pattern of the n_C = 18-cation exchanged material shows a 17.76 Å peak. The transition from the monolayer to the bilayer arrangement was achieved during a 5-day exchange procedure. Therefore, the time period of 20 min used for the 'on-grid exchange procedure' for TEM observations was probably too short and the interlayer charge too small in order to achieve a bilayer arrangement within the interlayer space of the low-charge saponite phases that formed during the synthesis. Crystals with greater interlayer charge (bilayer arrangement with 17.76 Å peak in XRD; Figure 7d) incorporate the n_C = 18 cations into a disordered paraffin-type arrangement causing a significant expansion of the interlayer space similar to the model of Lee and Kim (2002) (their figure 10d).

Rectorite. High-resolution lattice-fringe images of the rectorite after treatment with n_C = 18 cations also showed differences from the XRD pattern. The expandable 2:1 silicate layers of the rectorite behave similarly upon treatment with n_C = 18 cations in the ultrathin sections to the highly expanded saponite packets. The lattice-fringe images of the pure rectorite showed alternating sequences of expanded interlayers (26–28 Å) and non-expanded interlayers (~10 Å) (Figure 4d). The XRD pattern of the n_C = 18 cation exchanged rectorite has a first-order reflection at 27.33 Å which is caused by repeating coherent units that are composed of the non-expanded ~10 Å double layers and the expanded 17.33 Å low-charge 2:1 silicate layers (10 Å + 17.33 Å = 27.33 Å). However, the same unit measured in TEM lattice-fringe images would give 36 to 38 Å structures (*e.g.* 10 Å + 28 Å = 38 Å), an expansion of the low-charge silicate layers which is ~10 Å wider than in the XRD pattern (Figure 3c, 4d).

The comparison of lattice-fringe images of rectorite treated with n_C = 18 cations before embedding (Figure 1, method 2) with those of rectorite crystals on which the treatment was performed on the ultrathin sections, after embedding ('on-grid' exchange procedure; Figure 1, method 1), also supports the hypothesis of additional incorporation of *n*-alkylammonium cations in the low-charge interlayer. Ultrathin sections of rectorite treated with n_C = 18 cations after embedding showed an expansion of 26–28 Å for the low-charge interlayer (Figure 4d) while the same layers showed spacings of 17–21 Å in lattice-fringe images of rectorite treated with n_C = 18 cations before the embedding (Figure 10a–b). Only the outer low-charge layers of some sequences treated with n_C = 18 cations before the embedding show a wider expansion due to the intrusion of embedding resin into the interlayer space (Figure 10a: white arrows). The majority of the expanded interlayers in the inner parts of the rectorite crystals have spacings of 17–21 Å which suggests a bilayer to pseudotrimolecular arrangement of the n_C = 18 cations. These spacings, together with the non-expanded ~10 Å layers, would give a superlattice structure with spacings ranging from 27 to 31 Å (*e.g.* 10 Å + (17 to 21 Å) = 27 to 31 Å) which is close to the value obtained from the XRD analyses (27.33 Å) (Figures 3c, 10a,b).

The expandable interlayers of rectorite in experiment 2 (saponite-rectorite mixture) behave in a similar way. Lattice-fringe images show altered rectorite sequences having expanded interlayers up to 44 Å while the XRD patterns of the n_C = 18 cation-exchanged material show a broad first-order peak of rectorite with a maximum spacing of 32.82 Å. The alteration of the rectorite sequences due to the formation of talc and saponite proceeds along the low-charge interlayers of rectorite. Upon treatment with n_C = 18 cations the altered sequences incorporate more *n*-alkylammonium cations into the low-charge interlayer and, therefore, have a wider expansion (up to 44 Å) than the non-altered sequences (26–28 Å).

CONCLUSIONS

The results of the present study document the alteration of rectorite crystallites in a silicate gel with admixed oxalate due to the crystallization of saponite and talc from the gel. In the first experiment, the disodium oxalate solution was shown to alter the structure of rectorite at 60ºC and atmospheric pressure. Analysis by XRD and TEM suggest that excess Na^+ is first incorporated into the interlayer space of the low-charge rectorite layers causing a contraction of the structure and the development of a first-order reflection close to 10.20 Å. Upon treatment with EG or n_C = 18 cations, the dominant reflection at 10.20 Å disappeared. The cation exchange reaction with organic molecules generates the typical XRD pattern for rectorite.

https://doi.org/10.1346/CCMN.2013.0610413 Published online by Cambridge University Press

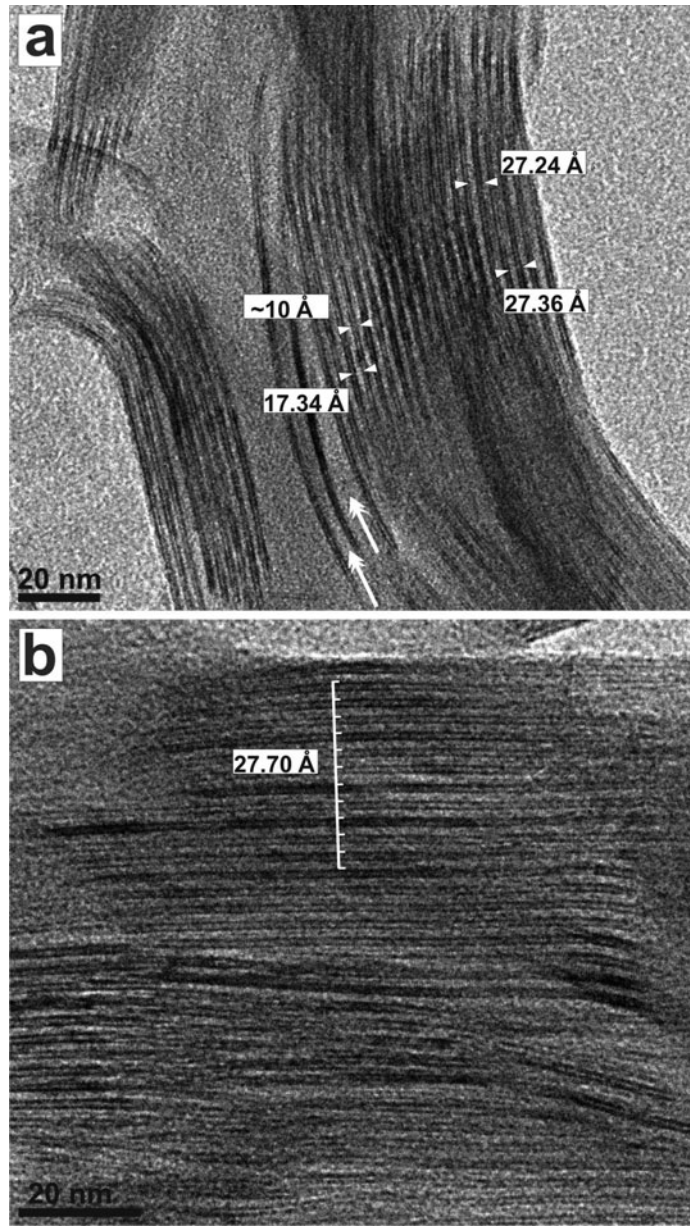

Figure 10. Lattice-fringe images of pure rectorite treated with $n_C = 18$ cations before embedding in EPON resin and ultrathin-section cutting (see method 2 in Figure 1): (a,b) sequences of expanded 17–21 Å layers alternating with non-expanded ~10 Å layers. The spacing of the non-expanded and expanded 2:1 silicate layers gives a value of 27–31 Å which is similar to the first-order reflection of n_C = 18-treated pure rectorite (Figure 3c). The expandable interlayers at the outer side of some of the rectorite crystals show additional expansion which is probably due to the intrusion of embedding resin (white arrows in part a).

The appearance of a reflection close to 14 Å in the air-dried sample suggested the formation of Al-hydroxy complexes, probably intercalated as discontinuous layers in some of the expandable rectorite interlayers. The Al may have been mobilized through complex formation with oxalate.

In the second experiment that contained silicate gel, rectorite, and disodium oxalate solution (under the same temperature and pressure conditions as in the first experiment), whether or not oxalate promotes the intercalation synthesis of new 2:1 silicate layers in the low-charge interlayers of rectorite was tested. The synthesis experiment produced globular aggregates of saponite crystals and fine talc crystallites. Saponite crystals and crystal aggregates occur separately from the rectorite but also use the rectorite crystals as nucleation sites. The edge sites of the rectorite crystals acted as nucleation sites for the very fine talc crystals. In many cases, the talc overgrowth completely covered the host rectorite crystals and even intruded into the interlayer

https://doi.org/10.1346/CCMN.2013.0610413 Published online by Cambridge University Press

space. The nucleation reaction of saponite released H^+ which could have reduced the pH and may have contributed to the alteration of the rectorite. Therefore, the nucleation of saponite and talc crystallites as well as the proton release associated with the saponite crystallization probably caused the destruction of the rectorite packages. The low-charge interlayer of rectorite does not act as a seed or template for the synthesis of new intercalation 2:1 silicate layers; instead, the newly formed saponite and talc crystallites grew in an irregular manner in the low-charge interlayers of rectorite causing an extreme expansion and, ultimately, destruction of the rectorite. Although the present study demonstrated that saponite 2:1 silicate layers did not intercalate in the expanding interlayers of rectorite under the selected experimental conditions, the possibility that new 2:1 silicate layers could form in expanding interlayers under other conditions is not excluded.

ACKNOWLEDGMENTS

C.G. Whitney is gratefully acknowledged for providing the synthetic silicate gel and Jeannie Mui and Lee Ann Monaghan of the Facility for Electron Microscopy Research are thanked for the preparation of ultrathin sections used in the HRTEM analysis. This work was supported by grants from the Natural Science and Engineering Research Council of Canada (H.V. and R.H.) and the Fonds Québécois de la Recherche sur la Nature et les Technologies to the Centre for Biorecognition and Biosensors (H.V.).

REFERENCES

Ahn, J.H. and Peacor, D.R. (1985) Transmission electron-microscopic study of diagenetic chlorite in Gulf-coast argillaceous sediments. *Clays and Clay Minerals*, **33**, 228–236.

Ahn, J.H. and Peacor, D.R. (1986) Transmission and analytical electron-microscopy of the smectite-to-illite transition. *Clays and Clay Minerals*, **34**, 165–179.

April, R.H., Hluchy, M.M., and Newton, R.M. (1986) The nature of vermiculite in Adirondack soils and till. *Clays and Clay Minerals*, **34**, 549–556.

Axe, K. and Persson, P. (2001) Time-dependent surface speciation of oxalate at the water-boehmite (γ-AlOOH) interface: Implications for dissolution. *Geochimica et Cosmochimica Acta*, **65**, 4481–4492.

Bain, D.C., Mellor, A., and Wilson, M.J. (1990) Nature and origin of an aluminous vermiculitic weathering product in acid soils from upland catchments in Scotland. *Clay Minerals*, **25**, 467–475.

Barnhisel, R.I. and Bertsch, P. (1989) Chlorites and hydroxy-interlayered vermiculite and smectite. Pp. 729–788 in: *Minerals in Soil Environments*. (J.B. Dixon and S.B. Weed, editors). Soil Science Society of America, Madison, Wisconsin, USA.

Barron, P.F., Slade, P., and Frost, R.L. (1985a) Solid-state SI-29 spin-lattice relaxation in several 2-1 phyllosilicate minerals. *Journal of Physical Chemistry*, **89**, 3305–3310.

Barron, P.F., Slade, P., and Frost, R.L. (1985b) Ordering of aluminum in tetrahedral sites in mixed-layer 2-1 phyllosilicates by solid-state high-resolution NMR. *Journal of Physical Chemistry*, **89**, 3880–3885.

Bell, T.E. (1986) Microstructure in mixed-layer illite smectite and its relationship to the reaction of smectite to illite. *Clays and Clay Minerals*, **34**, 146–154.

Bevan, J. and Savage, D. (1989) The effect of organic-acids on the dissolution of K-feldspar under conditions relevant to burial diagenesis. *Mineralogical Magazine*, **53**, 415–425.

Blake, R.E. and Walter, L.M. (1996) Effects of organic acids on the dissolution of orthoclase at 80ºC and pH 6. *Chemical Geology*, **132**, 91–102.

Boyle, J.R., Voigt, G.K., and Sawhney, B.L. (1967) Biotite flakes – alteration by chemical and biological treatment. *Science*, **155**, 193–195.

Bradley, W.F. (1950) The alternating layer sequence of rectorite. *American Mineralogist*, **35**, 590–595.

Brindley, G.W. (1956) Allevardite, a swelling double-layer mica mineral. *American Mineralogist*, **41**, 91–103.

Brindley, G.W. (1981) Structures and chemical composition of clay minerals. Pp. 1–21 in: *Short Course: Clays for the Resource Geologist* (F.J. Longstaffe, editor). International Clay Conference, Bologna and Pavia, Italy.

Brindley, G.W., Suzuki, T., and Thiry, M. (1983) Interstratified kaolinite smectites from the Paris basin – correlations of layer proportions, chemical-compositions and other data. *Bulletin de Mineralogie*, **106**, 403–410.

Brown, G. and Weir, A.H. (1965) The identity of rectorite and allevardite. *Proceedings of the International Clay Conference Stockholm*. (I.T. Rosenqvist and P. Graff-Petersen), Pergamon, Oxford, UK, pp. 27–35.

Burst, J.F. (1959) Post diagenetic clay mineral-environmental relationships in the Gulf Coast Eocene in clays and clay minerals. *Clays and Clay Minerals*, **6**, 327–41.

Burst, J.F. (1969) Diagenesis of Gulf Coast clayey sediments and its possible relation to petroleum migration. *American Association of Petroleum Geologists Bulletin*, **53**, 73–93.

Caillère, S. and Hénin, S. (1949) Transformation of minerals of the montmorillonite family into 10 Å micas; and experimental formation of chlorites from montmorillonite. *Mineralogical Magazine*, **28**, 606–620.

Caillère, S., Hénin, S., and Esquevin, J. (1953) Synthesis of clay minerals. *Bulletin de la Societé Française de Mineralogie et Cristallographie*, **76**, 300–314.

Couturier, Y., Michard, G., and Sarazin, G. (1984) Stability-constants of aluminum hydroxo complexes in aqueous-solutions at 20–70ºC. *Geochimica et Cosmochimica Acta*, **48**, 649–659.

Crossey, L.J. (1991) Thermal-degradation of aqueous oxalate species. *Geochimica et Cosmochimica Acta*, **55**, 1515–1527.

Dean, R.S. (1983) Authigenic trioctahedral clay minerals coating Clearwater Formation sand grains at Cold Lake, Alberta, Canada. Program with abstracts: 20th Annual Meeting, The Clay Minerals Society, Buffalo, New York, USA, p. 79.

Dobson, K.D. and McQuillan, A.J. (1999) In situ infrared spectroscopic analysis of the adsorption of aliphatic carboxylic acids to TiO_2, ZrO_2, Al_2O_3, and Ta_2O_5 from aqueous solutions. *Spectrochimica Acta Part A – Molecular and Biomolecular Spectroscopy*, **55**, 1395–1405.

Duckworth, O.W. and Martin, S.T. (2001) Surface complexation and dissolution of hematite by C-1-C-6 dicarboxylic acids at pH = 5.0. *Geochimica et Cosmochimica Acta*, **65**, 4289–4301.

Farmer, V.C., Smith, B.F.L., Wilson, M.J., Loveland, P.J., and Payton, R.W. (1988) Readily-extractable hydroxyaluminum interlayers in clay-sized and silt-sized vermiculite. *Clay Minerals*, **23**, 271–277.

Fein, J.B. (1991) Experimental-study of aluminum-oxalate complexing at 80ºC – implications for the formation of secondary porosity within sedimentary reservoirs. *Geology*, **19**, 1037–1040.

Fein, J.B. and Brady, P.V. (1995) Mineral surface controls on

the diagenetic transport of oxalate and aluminum. *Chemical Geology*, **121**, 11–18.

Fein, J.B. and Hestrin, J.E. (1994) Experimental studies of oxalate complexation at 80ºC: Gibbsite, amorphous silica, and quartz solubilities in oxalate-bearing fluids. *Geochimica et Cosmochimica Acta*, **58**, 4817–4829.

Gruner, J.W. (1934) The structures of vermiculites and their collapse by dehydration. *American Mineralogist*, **19**, 557–575.

Güven, N. (1991) On a definition of illite smectite mixed-layer. *Clays and Clay Minerals*, **39**, 661–662.

Hamilton, D.L. and Henderson, C.M.B. (1968) The preparation of silicate compositions by a gelling method. *Mineralogical Magazine*, **36**, 832–838.

He, H., Frost, R.L., Deng, F., Zhu, J., Wen, X., and Yuan, P. (2004) Conformation of surfactant molecules in the interlayer of montmorillonite studied by 13C MAS NMR. *Clays and Clay Minerals*, **52**, 350–356.

He, H., Ding, Z., Zhu, J., Yuan, P., Xi, Y., Yang, D., and Frost, R.L. (2005) Thermal characterization of surfactant-modified montmorillonites. *Clays and Clay Minerals*, **53**, 287–293.

He, H.P., Zhou, Q., Martens, W.N., Kloprogge, T.J., Yuan, P., Yunfei, X.F., Zhu, J.X., and Frost, R.L. (2006) Microstructure of HDTMA(+)-modified montmorillonite and its influence on sorption characteristics. *Clays and Clay Minerals*, **54**, 689–696.

Henderson, G.V. (1970) The origin of pyrophyllite rectorite in shales of north central Utah. *Clays and Clay Minerals*, **18**, 239–246.

Hénin, S. and Robichet, O. (1954) A study of the synthesis of clay minerals. *Clay Minerals*, **2**, 110–115.

Hower, J., Eslinger, E.V., Hower, M.E., and Perry, E.A. (1976) Mechanism of burial metamorphism of argillaceous sediment: mineralogical and chemical evidence. *Geological Society of America Bulletin*, **87**, 725–737.

Hughes, R.E., Moore, D.M., and Reynolds, R.C., Jr. (1993) The nature, detection, and occurence, and origin of kaolinite/smectite. Pp. 291–323 in: *Kaolin Genesis and Utilization* (H.H. Murray, W.M. Bundy and C.C. Harvey, editors). The Clay Minerals Society, Boulder, Colorado, USA.

Jakobsen, H.J., Nielsen, N.C., and Lindgreen, H. (1995) Sequences of charged sheets in rectorite. *American Mineralogist*, **80**, 247–252.

Koehler, S.J., Dufaud, F., and Oelkers, E.H. (2003) An experimental study of illite dissolution kinetics as a function of pH from 1.4 to 12.4 and temperature from 5 to 50 degrees C. *Geochimica et Cosmochimica Acta*, **67**, 3583–3594.

Lagaly, G. (1979) Layer charge of regular interstratified 2:1 clay minerals. *Clays and Clay Minerals*, **27**, 1–10.

Lagaly, G. (1981) Inorganic layer compounds – phenomena of interface reactions with organic compounds. *Naturwissenschaften*, **68**, 82–88.

Lagaly, G. (1982) Layer charge heterogeneity in vermiculites. *Clays and Clay Minerals*, **30**, 215–222.

Lagaly, G. and Dékany, I. (2005) Adsorption on hydrophobized surfaces: Clusters and self-organization. *Advances in Colloid and Interface Science*, **114–115**, 189–204.

Lagaly, G. and Weiss, A. (1969) Determination of layer charge in mica-type layer silicates. *Proceedings of the International Clay Conference, Tokyo*, pp. 61–80.

Lagaly, G. and Weiss, A. (1970a) Arrangement and orientation of cationic surfactants on plane silicate surfaces. 1. Preparation of normal-alkylammonium derivates of mica type laminated silicates. *Kolloid-Zeitschrift und Zeitschrift für Polymere*, **237**, 266–273.

Lagaly, G. and Weiss, A. (1970b) Arrangement and orientation of cationic tensides on silicate surfaces. 2. Paraffin-like structures in alkylammonium layer silicates with high layer charge (mica). *Kolloid-Zeitschrift und Zeitschrift für Polymere*, **237**, 364–368.

Lagaly, G. and Weiss, A. (1970c) Arrangement and orientation of cationic tensides on silicate surfaces. 3. Paraffin-like structures in alkylammonium layer silicates with an average layer load (vermiculite). *Kolloid-Zeitschrift und Zeitschrift für Polymere*, **238**, 485–493.

Lee, S.Y. and Kim, S.J. (2002) Expansion of smectite by hexadecyltrimethylammonium. *Clays and Clay Minerals*, **50**, 435–445.

MacEwan, D.M.C. (1949) Some notes on the recording and interpretation of X-ray diagrams of soil clays. *Journal of Soil Science*, **1**, 90–103.

Maes, A., Stul, M.S., and Cremers, A. (1979) Layer charge-cation-exchange capacity relationships in montmorillonite. *Clays and Clay Minerals*, **27**, 387–392.

Malla, P.B. and Douglas, L.A. (1987) Identification of expanding layer silicates: layer charge vs. expansion properties. International Clay Conference, Denver, The Clay Minerals Society, Bloomington, Indiana, USA, pp. 277–283.

Meunier, A. (2007) Soil hydroxy-interlayered minerals: A re-interpretation of their crystallochemical properties. *Clays and Clay Minerals*, **55**, 380–388.

Moore, D.M., Ahmed, J., and Grathoff, G. (1989) Mineralogy of the Eocene Ghazij Shale, Western Indus Basin, Pakistan. Program with Abstracts: 9th International Clay Conference, Strasbourg, France, p. 266.

Nadeau, P.H., Wilson, M.J., McHardy, W.J., and Tait, J.M. (1984) Interstratified clays as fundamental particles. *Science*, **225**, 923–925.

Nadeau, P.H., Wilson, M.J., McHardy, W.J., and Tait, J.M. (1985) The conversion of smectite to illite during diagenesis – evidence from some illitic clays from bentonites and sandstones. *Mineralogical Magazine*, **49**, 393–400.

Perry, E. and Hower, J. (1970) Burial diagenesis in Gulf Coast pelitic sediments. *Clays and Clay Minerals*, **18**, 165–177.

Perry, E.A. and Hower, J. (1972) Late-stage dehydration in deeply buried pelitic sediments. *American Association of Petroleum Geologists Bulletin*, **56**, 2013–2021.

Powers, M.C. (1967) Fluid-release mechanisms in compacting marine mudrocks and their importance in oil exploration. *American Association of Petroleum Geologists Bulletin*, **51**, 1240–1254.

Reynolds, R.C. and Hower, J. (1970) The nature of interlayering in mixed-layer illite-montmorillonites. *Clays and Clay Minerals*, **18**, 25–36.

Rich, C.I. (1968) Hydroxy interlayers in expansible layer silicates. *Clays and Clay Minerals*, **16**, 15–30.

Schumann, D., Hartman, H., Eberl, D.D., Sears, S.K., Hesse, R., and Vali, H. (2012) Formation of replicating saponite from a gel in the presence of oxalate: Implications for the formation of clay minerals in carbonaceous chondrites and the origin of life. *Astrobiology*, **12**, 549–561.

Sears, S.K., Hesse, R., Vali, H., Elliott, W.C., and Aronson, J.L. (1995) K-Ar dating of illite diagenesis in ultrafine fractions of mudrocks from the Reindeer D-27 well, Beaufort-Mackenzie area, Arctic Canada. 8th International Symposium on Water–Rock Interaction Vladivostok, pp. 105–108.

Sears, S.K., Hesse, R., and Vali, H. (1998) Significance of n-alkylammonium exchange in the study of 2:1 clay mineral diagenesis, Mackenzie Delta Beaufort Sea region, Arctic Canada. *The Canadian Mineralogist*, **36**, 1485–1506.

Shata, S., Hesse, R., Martin, R.F., and Vali, H. (2003) Expandability of anchizonal illite and chlorite: Significance for crystallinity development in the transition from diagenesis to metamorphism. *American Mineralogist*, **88**, 748–762.

Sherman, D.M. and Randall, S.R. (2003) Surface complexation of arsenic(V) to iron(III) (hydr)oxides: Structural mechanism from ab initio molecular geometries and EXAFS spectroscopy. *Geochimica et Cosmochimica Acta*, **67**, 4223–4230.

Środoń, J. (1999) Nature of mixed-layer clays and mechanisms of their formation and alteration. *Annual Review of Earth and Planetary Sciences*, **27**, 19–53.

Środoń, J. and Eberl, D.D. (1984) Illite. Pp. 495–544 in: *Micas* (S.W. Bailey, editor). Reviews in Mineralogy, **13**, Mineralogical Society of America, Washington, D.C.

Stillings, L.L., Drever, J.I., and Poulson, S.R. (1998) Oxalate adsorption at a plagioclase (An_{47}) surface and models for ligand-promoted dissolution. *Environmental Science & Technology*, **32**, 2856–2864.

Stoessell, R.K. and Pittman, E.D. (1990) Secondary porosity revisited – the chemistry of feldspar dissolution by carboxylic-acids and anions. *American Association of Petroleum Geologists Bulletin*, **74**, 1795–1805.

Sudo, T., Takahashi, H., and Matsui, H. (1954) A long spacing at about 30-KX confirmed from a fireclay. *Nature*, **173**, 261–262.

Surdam, R.C. and MacGowan, D.B. (1978) Oilfield waters and sandstone diagenesis. *Applied Geochemistry*, **2**, 613–619.

Tait, C.D., Janecky, D.R., Clark, D.L., and Bennett, P.C. (1992) Oxalate complexation of aluminum (III) and iron (III) at moderately elevated temperatures. Pp. 349–352 in: *Water–Rock Interaction 7* (Y.K. Kharaka and A.S. Maest, editors). Balkema, Rotterdam.

Thyne, G.D., Harrison, W.J., and Alloway, M.D. (1992) Experimental study of the stability of the Al-oxalate complex at 100ºC and calculations of the effects of complexation on clastic diagenesis. Pp. 353–357 in: *Water-Rock Interaction 7* (Y.K. Kharaka and A.S. Maest, editors). Balkema, Rotterdam.

Vali, H. and Hesse, R. (1990) Alkylammonium treatment of clay minerals in ultrathin sections – A new method for HRTEM examination of expandable layers. *American Mineralogist*, **75**, 1443–1446.

Vali, H. and Hesse, R. (1992) Identification of vermiculite by transmission electron microscopy and X-ray diffraction. *Clay Minerals*, **27**, 185–192.

Vali, H. and Köster, H. M. (1986) Expanding behavior, structural disorder, regular and random irregular interstratification of 2:1 layer silicates studied by high resolution images of transmisson electron microscopy. *Clay Minerals*, **21**, 827–859.

Vali, H., Hesse, R., and Kohler, E.E. (1991) Combined freeze-etch replicas and HRTEM images as tools to study fundamental particles and the multiphase nature of 2:1 layer silicates. *American Mineralogist*, **76**, 1973–1984.

Vali, H., Hesse, R., and Martin, R.F. (1994) A TEM-based definition of 2:1 layer silicates and their interstratified constituents. *American Mineralogist*, **79**, 644–653.

Weiss, A. (1981) Replication and evolution in inorganic systems. *Angewandte Chemie-International Edition in English*, **20**, 850–860.

Welch, S.A. and Ullman, W.J. (1996) Feldspar dissolution in acidic and organic solutions: Compositional and pH dependence of dissolution rate. *Geochimica et Cosmochimica Acta*, **60**, 2939–2948.

White, G.N. and Zelazny, L.W. (1988) Analysis and implications of the edge structure of dioctahedral phyllosilicates. *Clays and Clay Minerals*, **36**, 141–146.

Whitney, G. (1983) Hydrothermal reactivity of saponite. *Clays and Clay Minerals*, **31**, 1–8.

Yoon, T.H., Johnson, S.B., Musgrave, C.B., and Brown, G.E. (2004) Adsorption of organic matter at mineral/water interfaces: I. ATR-FTIR spectroscopic and quantum chemical study of oxalate adsorbed at boehmite/water and corundum/water interfaces. *Geochimica et Cosmochimica Acta*, **68**, 4505–4518.

Zhu, J.X., He, H.P., Guo, J.G., Yang, D., and Xie, X.D. (2003) Arrangement models of alkylammonium cations in the interlayer of HDTMA(+) pillared montmorillonites. *Chinese Science Bulletin*, **48**, 368–372.

(*Received 19 November 2012; revised 3 August 2013; Ms 726; AE: M. Kawano*)